Chapter

Magnetic Full-Heusler Compounds for Thermoelectric Applications

Kei Hayashi, Hezhang Li, Mao Eguchi, Yoshimi Nagashima and Yuzuru Miyazaki

Abstract

Full-Heusler compounds exhibit a variety of magnetic properties such as non-magnetism, ferromagnetism, ferrimagnetism and anti-ferromagnetism. In recent years, they have attracted significant attention as potential thermoelectric (TE) materials that convert thermal energy directly into electricity. This chapter reviews the theoretical and experimental studies on the TE properties of magnetic full-Heusler compounds. In Section 1, a brief outline of TE power generation is described. Section 2 introduces the crystal structures and magnetic properties of full-Heusler compounds. The TE properties of full-Heusler compounds are presented in Sections 3 and 4. The relationship between magnetism, TE properties and order degree of full-Heusler compounds is elaborated.

Keywords: full-Heusler compounds, half-metal, spin-gapless semiconductor, thermoelectric properties, order degree

1. Introduction

Thermoelectric (TE) power generation using TE devices is one of the key technologies to solve global energy problem, owing to its availability of direct conversion of thermal energy into electricity [1–3]. A schematic figure of a TE device is shown in **Figure 1**. It consists of n- and p-type TE materials connected in series electrically with metal electrodes and arranged thermally in parallel. The TE materials are wedged between ceramic plates. When one side of the device is heated and the other side is cooled, electrons and holes in the n- and p-type TE materials, respectively, diffuse from the hot side to the cold side, thus generating a flow of electric current.

To commercialise TE devices, there is a need to improve their TE efficiency. The maximum TE efficiency, η_{max}, is an increasing function of the dimensionless figure-of-merit, zT, expressed as:

$$\eta_{\mathrm{max}} = \frac{T_{\mathrm{H}} - T_{\mathrm{C}}}{T_{\mathrm{H}}} \frac{\sqrt{1+zT} - 1}{\sqrt{1+zT} + T_{\mathrm{C}}/T_{\mathrm{H}}}, \quad (1)$$

where T_{H} and T_{C} are the heating and cooling temperature, respectively. The dimensionless figure-of-merit, zT, is determined by TE properties (S: Seebeck

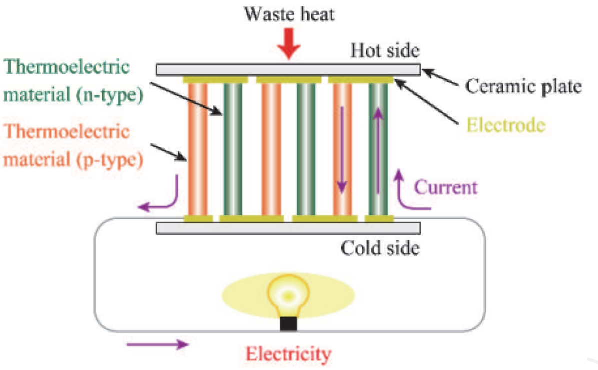

Figure 1.
Schematic figure of a thermoelectric (TE) power generation device.

coefficient, σ: electrical conductivity, κ: thermal conductivity) of the individual TE materials in the device.

$$zT = \frac{S^2\sigma}{\kappa}T, \tag{2}$$

where T is the absolute temperature. The product $S^2\sigma$ is called the power factor (PF), which is a measure of electric power generated using the TE material. To achieve high TE efficiency (standard levels for practical use are $zT > 1$ and $\mathrm{PF} > 2 \times 10^{-3}$ W/K^{2}m), high S, high σ and low κ are required. To meet these requirements, a variety of TE materials have been explored, such as chalcogenides, skutterudites, clathrates, silicides, Zintl compounds, half-Heusler compounds and oxides [1–3]. Most of these materials are semiconductors because in general they have high S than metals. However, recent theoretical and experimental studies have revealed that metals, in particular, half-metallic full-Heusler compounds have relatively high S as well as high σ. In addition, their junction with a metal electrode is robust compared to that of semiconductors, which is also an advantage.

In Section 2, the crystal structures and magnetic properties of full-Heusler compounds are introduced. Sections 3 and 4 demonstrate that magnetic full-Heusler compounds are promising for the TE power generation device.

2. Crystal structures and magnetic properties of full-Heusler compounds

The physical properties of full-Heusler compounds depend on their crystal structures. As shown in **Figure 2**, there are several types of crystal structures with different order degrees [4–6]. The full-Heusler compounds have four interpenetrating fcc sublattices, and each sublattice consists of the X, X', Y or Z atom. The X, X' and Y atoms are transition metals, whereas Z is a main group element. In some cases, the Y atom is a rare earth element or an alkaline earth metal.

When the X and X' atoms are of the same element, the chemical composition of the compounds is written as X_2YZ, which generally crystallises in the $L2_1$ structure. The prototype of the $L2_1$ structure is Cu_2MnAl (space group: $Fm\bar{3}m$). The Cu atoms occupy the 8c (1/4 1/4 1/4) site, whereas the Mn and Al atoms occupy the 4b (1/2 1/2 1/2) and 4a (0 0 0) sites, respectively. The $L2_1$ structure is a highly ordered structure of the full-Heusler compounds. Disorder among the Cu, Mn and/or Al atoms, that is, antisite defects, gives rise to different crystal structures. In a case where the Mn and Al atoms are evenly located at the 4b and 4a sites, the Cu_2MnAl becomes the B2 structure. Its prototype is CsCl (space group: $Pm\bar{3}m$). In a fully

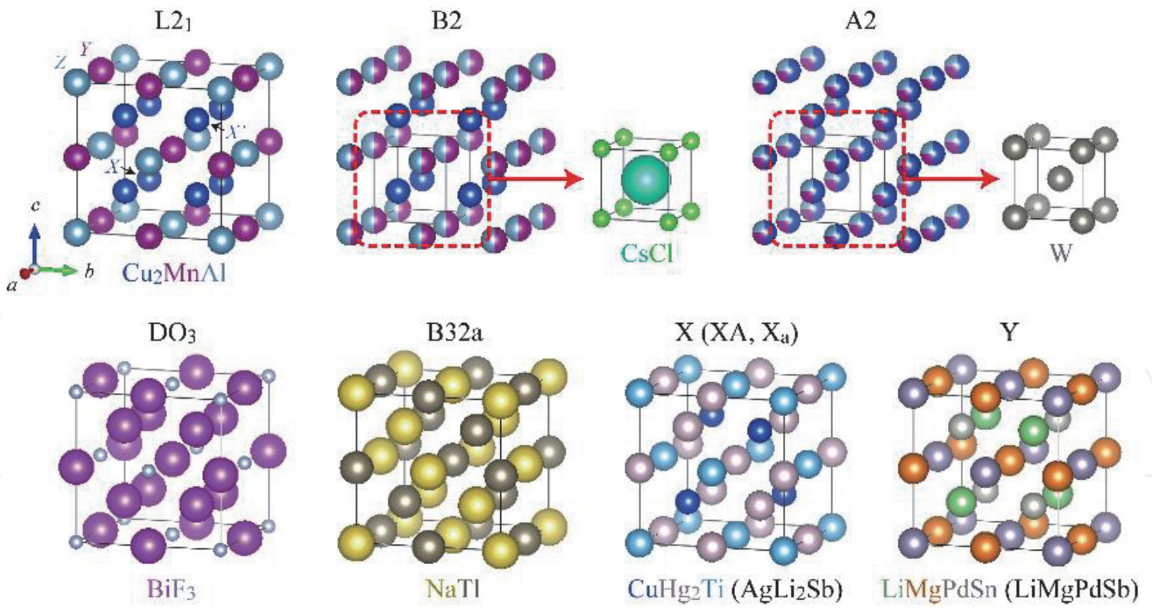

Figure 2.
Crystal structures of full-Heusler compounds. The Strukturbericht symbol and a prototype structure are written above and below each crystal structure, respectively.

disordered phase, all the atoms are randomly distributed in the 8*c*, 4*b* and 4*a* sites, thus resulting in the A2 structure. In such a structure, all the sites are equivalent, which are expressed as a bcc lattice (prototype: W, space group: $Im\bar{3}m$). There are other disordered phases, including the DO_3 and B32a structures. The former is caused by the random distribution of the *X*, *X'* and *Y* atoms at the 8*c* and 4*b* sites (prototype: BiF_3, space group: $Fm\bar{3}m$). In the B32a structure, the 8*a* (0 0 0) and 8*b* (1/2 1/2 1/2) sites are occupied by the *X*/*Y* and *X'*/*Z* atoms, respectively. The prototype is NaTl (space group: $Fd\bar{3}m$).

When the *X'* and *Y* atoms are of the same element, the chemical composition becomes XX'_2Z, which crystallises in the X (XA or X_a) structure. This structure is called the inverse Heusler phase. The prototype is $CuHg_2Ti$ (or $AgLi_2Sb$), and the space group is $F\bar{4}3\,m$. In the structure, the *X* and *Z* atoms occupy the 4*d* (3/4 3/4 3/4) and 4*a* (0 0 0) sites, respectively, and the *X'* atoms occupy the 4*b* (1/2 1/2 1/2) and 4*c* (1/4 1/4 1/4) sites.

In addition to the above ternary full-Heusler compounds, there are quaternary full-Heusler compounds, *XX'YZ*, which crystallise in the *Y* structure (prototype: LiMgPdSn or LiMgPdSb, space group: $F\bar{4}3\,m$). The *X*, *X'*, *Y* and *Z* atoms are situated at the 4*d*, 4*b*, 4*c* and 4*a* sites, respectively, occupying one of the fcc sublattices. It should be noted that the inverse Heusler and the quaternary full-Heusler phases are ordered phases, and any disorder among the constituent atoms causes a structural change; the structure changes to the B2, A2, DO_3 or B32a structure.

Earlier theoretical studies demonstrated a half-metallic nature in full-Heusler compounds [7, 8]. Since then, many studies have been dedicated to investigate the electronic and magnetic properties of ternary and quaternary full-Heusler compounds. It has been revealed that full-Heusler compounds exhibit a variety of electronic properties; they exhibit the properties of semiconductors [9–18], spin-gapless semiconductors (SGSs) [19–26], semimetals [27–29], metals [30–34] and half-metals (HMs) [32, 35–78]. Considering the magnetic properties, they have been reported to exhibit nonmagnetism [9–11, 14–18], ferromagnetism [12, 19–24, 30–33, 36–46, 48–58, 61–66, 68–78], ferrimagnetism [13, 30, 35, 47, 59, 60, 67] and antiferromagnetism [25, 26, 34]. The full-Heusler, inverse Heusler and quaternary Heusler compounds obey the Slater-Pauling rule [79–81]: the total spin magnetic moment per unit cell scales with the total number of valence electrons in the unit cell.

3. Thermoelectric properties of half-metallic full-Heusler compounds

In this section, we present some of the theoretical and experimental studies on the TE properties of half-metallic full-Heusler compounds. The TE properties can be calculated on the basis of the Boltzmann transport equations [82–84]. Using the electronic energy-wavenumber dispersion curve of the i-th band $\varepsilon_i(\boldsymbol{k})$, the tensors of the Seebeck coefficient, $\boldsymbol{S}(T)$, electrical conductivity, $\boldsymbol{\sigma}(T)$, and carrier thermal conductivity, $\boldsymbol{\kappa}_{\mathrm{e}}(T)$, can be expressed as:

$$\boldsymbol{S}(T) = -\frac{1}{|e|T}\frac{\int_{-\infty}^{+\infty}\tilde{\boldsymbol{\sigma}}(\varepsilon,T)(\varepsilon-\varepsilon_{\mathrm{F}})\left(-\frac{\partial f_{\mathrm{FD}}(\varepsilon,T)}{\partial\varepsilon}\right)\mathrm{d}\varepsilon}{\boldsymbol{\sigma}(T)}, \tag{3}$$

$$\boldsymbol{\sigma}(T) = \int_{-\infty}^{+\infty}\tilde{\boldsymbol{\sigma}}(\varepsilon,T)\left(-\frac{\partial f_{\mathrm{FD}}(\varepsilon,T)}{\partial\varepsilon}\right)\mathrm{d}\varepsilon, \tag{4}$$

$$\begin{aligned}\boldsymbol{\kappa}_{\mathrm{e}}(T) = &-\frac{1}{e^2T}\int_{-\infty}^{+\infty}\tilde{\boldsymbol{\sigma}}(\varepsilon,T)(\varepsilon-\varepsilon_{\mathrm{F}})^2\left(-\frac{\partial f_{\mathrm{FD}}(\varepsilon,T)}{\partial\varepsilon}\right)\mathrm{d}\varepsilon\\ &-\frac{1}{e^2T}\frac{\left\{\int_{-\infty}^{+\infty}\tilde{\boldsymbol{\sigma}}(\varepsilon,T)(\varepsilon-\varepsilon_{\mathrm{F}})\left(-\frac{\partial f_{\mathrm{FD}}(\varepsilon,T)}{\partial\varepsilon}\right)\mathrm{d}\varepsilon\right\}^2}{\boldsymbol{\sigma}(T)},\end{aligned} \tag{5}$$

$$\tilde{\sigma}_{\alpha\beta}(\varepsilon,T) \equiv \frac{1}{N_k}\sum_{i,k}\frac{e^2\tau(k,T)}{\hbar^2}\frac{\partial\varepsilon_i(k)}{\partial k_\alpha}\frac{\partial\varepsilon_i(k)}{\partial k_\beta}\delta(\varepsilon-\varepsilon_i(k)), (\alpha,\beta = x,y,z), \tag{6}$$

where e, ε, ε_{F}, $f_{\mathrm{FD}}(\varepsilon,T)$, N_k, $\tau(k,T)$, and $\tilde{\boldsymbol{\sigma}}(\varepsilon,T)$ are the elementary charge, electron energy, Fermi level, Fermi-Dirac distribution function, total number of the k-points, relaxation time, Dirac constant and conductance spectrum tensor, respectively. It is difficult to calculate the relaxation time; hence, the calculation of TE properties generally gives $\boldsymbol{S}(T)$, $\boldsymbol{\sigma}(T)/\tau$ and $\boldsymbol{\kappa}_{\mathrm{e}}(T)/\tau$ [84]. In context to magnetic materials, the electronic states of the majority and minority spin electrons are considered. Assuming that τ for the majority and minority spin electrons is the same, the total S for the magnetic materials, $S_{\mathrm{tot}}(T)$, is calculated by

$$S_{\mathrm{tot}}(T) = \frac{S_\uparrow(T)\sigma_\uparrow(T)/\tau + S_\downarrow(T)\sigma_\downarrow(T)/\tau}{\sigma_\uparrow(T)/\tau + \sigma_\downarrow(T)/\tau} = \frac{S_\uparrow(T)\sigma_\uparrow(T) + S_\downarrow(T)\sigma_\downarrow(T)}{\sigma_\uparrow(T) + \sigma_\downarrow(T)}, \tag{7}$$

where S and σ with the up- and down-arrow subscripts those evaluated from the electronic states of the majority and minority spin electrons, respectively.

Figure 3(a) and **(b)** shows the temperature dependence of the calculated S_{tot} for ternary and quaternary half-metallic full-Heusler compounds, respectively. To calculate the electronic band, the full-potential linearised augmented plane wave (FLAPW) method was employed, adopting the local spin density approximation (LSDA) or the generalised gradient approximation in the Perdew-Burke-Ernzerhof parametrisation (PBE-GGA) as the local exchange-correlation potential. As seen in the figure, the negative and positive S_{tot} are presented, indicating that both n-type and p-type materials can be obtained from half-metallic full-Heusler compounds. The S_{tot} is observed to increase with increasing temperature for almost all the compounds, which is the typical behaviour of metal. Furthermore, the S_{tot} is observed to attain values as high as several tens of μV/K. These values are lower

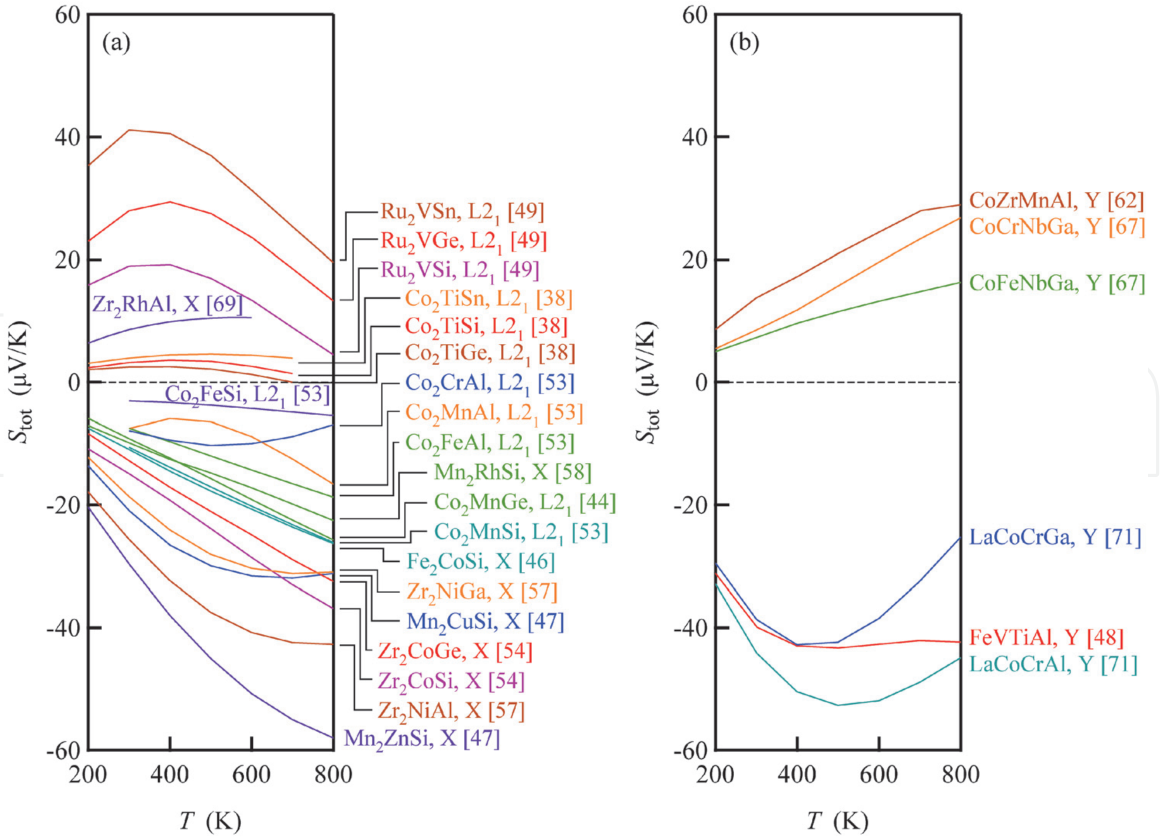

Figure 3.
Temperature dependence of the calculated S_{tot} for half-metallic full-Heusler compounds. Their crystal structures are also shown. The calculation of the electronic structure was performed using the full-potential linearised augmented plane wave (FLAPW) method with local spin density approximation (LSDA) or generalised gradient approximation in the Perdew-Burke-Ernzerhof parametrisation (PBE-GGA).

than those of TE semiconductors but higher than those of common metals, demonstrating the potential of half-metallic full-Heusler compounds as high-temperature TE materials.

The temperature dependence of S for several half-metallic Co-based full-Heusler compounds was determined by Balke et al. [37] and Hayashi et al. [53]. For the measurements, the S_{tot} values for the compounds were obtained. Hereafter, we use S to represent S_{tot}. As shown in **Figure 4(a)–(c)**, the Co-based full-Heusler compounds exhibit negative S in the order of several tens of μV/K. For metals, the sign of S is well explained by Mott's formula [85]:

$$S \propto -\frac{1}{\mathrm{DOS}(\varepsilon_F)} \frac{\mathrm{d\,DOS}(\varepsilon)}{\mathrm{d}\varepsilon}\bigg|_{\varepsilon=\varepsilon_F}, \tag{8}$$

where DOS is the electronic density of states. Adopting Eq. (8) for the partial DOS of the *sp*-electrons and *d*-electrons of Co_2MnSi, it was obtained that in half-metallic full-Heusler compounds, the itinerant *sp*-electrons contribute more to S than the localised *d*-electrons [53]. In **Figure 4**, Co_2TiAl is shown to exhibit the highest $|S|$ of $|-56|$ μV/K at 350 K among other compounds. It is observed that Co_2TiSi, Co_2TiGe and Co_2TiSn exhibit a characteristic temperature dependence of $|S|$; the value of $|S|$ increases with increasing temperature and becomes constant at temperatures above 350 K. This characteristic behaviour is further discussed later in this section.

The half-metallic full-Heusler compounds are predicted to have high electrical conductivity σ owing to their metallic properties; hence, they are considered to be superior to the semiconductors. **Figure 5(a)** shows the temperature dependence of

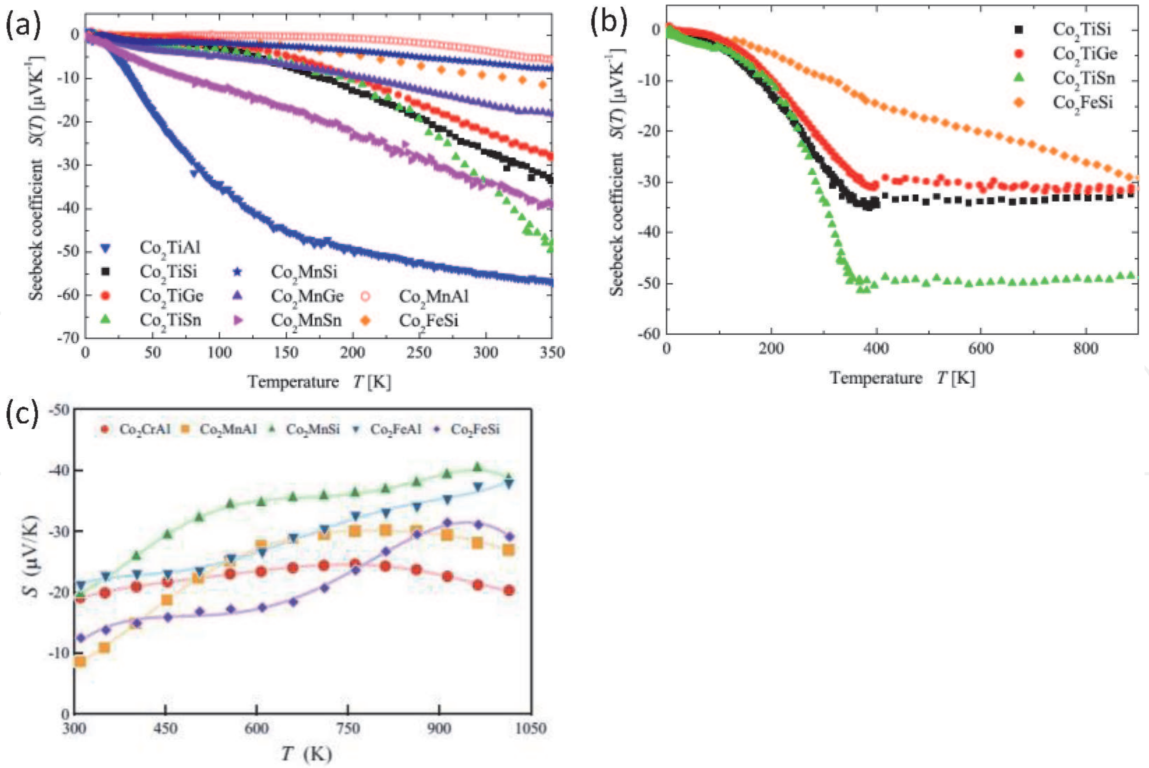

Figure 4.
Temperature dependence of the measured S *of several Co-based full-Heusler compounds. ((a) and (b) Reprinted from [37]. Copyright 2010, with permission from Elsevier. (c) Reprinted from [53]. Copyright 2017, with permission from Springer).*

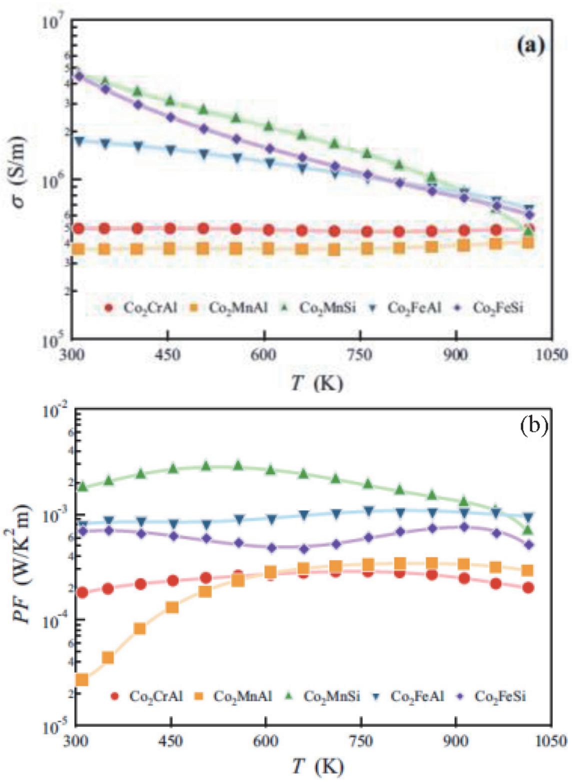

Figure 5.
(a) Measured σ *and (b) PF of several Co-based full-Heusler compounds as a function of temperature. (Reprinted from [53]. Copyright 2017, with permission from Springer).*

the measured σ for several Co-based full-Heusler compounds [53]. The σ values of the compounds are observed to be high, ranging from 10^5 to 10^7 S/m. Among all the compounds, Co_2MnSi exhibits the highest σ in the whole temperature range. The σ

value of Co_2MnSi decreases from 4.6×10^6 S/m at 300 K to 4.7×10^5 S/m at 1000 K. This is a typical electrical conductivity-temperature relation in metals. From the S and σ values (shown in **Figures 4(c)** and **5(a)**, respectively), the PF was calculated and plotted in **Figure 5(b)** [53]. Owing to the high S and high σ, Co_2MnSi exhibits the highest PF (2.9×10^{-3} W/K^{2}m at 500 K) among other compounds, which is comparable to that of a Bi_2Te_3-based material [86]. Since Co_2MnSi exhibits a negative S, it could be a potential n-type TE material. Thus, to develop a TE device using full-Heusler compounds, a p-type counterpart to Co_2MnSi is needed. For this purpose, Li et al. [60, 78] prepared a half-metallic Mn_2VAl compound and measured its TE properties. Although Mn_2VAl is a p-type material showing positive S, its highest PF (2.84×10^{-4} W/K^{2}m at 767 K [78]) is lower than that of Co_2MnSi. Thus, there is a need to explore more p-type half-metallic full-Heusler compounds with high PF.

Here, the temperature dependence of S for the various full-Heusler compounds is discussed. Comparing the calculated S values for Co_2TiSi, Co_2TiGe and Co_2TiSn (**Figure 3(a)**) with the measured values (**Figure 5(b)**), it is obtained that not only the temperature dependence but also the sign of the S values are different. As mentioned earlier, the measured S value is almost constant at temperatures above 350 K; however, the calculated values do not display such relation. To explain this difference, Barth et al. [38] considered the difference in the electronic structure of the ferromagnetic (FM) state and nonmagnetic (NM) states. They obtained that the FM-NM phase transition occurs around 350 K for Co_2TiSi, Co_2TiGe and Co_2TiSn [38]. Using the temperature dependence of S for the FM and NM states, $S_{\mathrm{FM}}(T)$ and $S_{\mathrm{NM}}(T)$, and that of the normalised magnetisation calculated by using the molecular field theory, $M(T)$, a modified S value, $S_{\mathrm{FM+NM}}$, can be calculated according to the formula [38]:

$$S_{\mathrm{FM+NM}}(T) = \frac{S_{\mathrm{FM}}(T)\sigma_{\mathrm{FM}}(T)M(T) + S_{\mathrm{NM}}(T)\sigma_{\mathrm{NM}}(T)\{1 - M(T)\}}{\sigma_{\mathrm{FM+NM}}(T)}, \qquad (9)$$

where $\sigma_{\mathrm{FM+NM}}$ is the modified electrical conductivity of a mixture of FM and NM states weighted by using $M(T)$. Although the above consideration is plausible, the calculated $S_{\mathrm{FM+NM}}$ values for Co_2TiSi, Co_2TiGe and Co_2TiSn (**Figure 6**) do not coincide with the measured values. The inconsistency between the $S_{\mathrm{FM+NM}}$ values and the measured ones is also observed in the case of Co_2CrAl, Co_2MnAl, Co_2MnSi, Co_2FeAl and Co_2FeSi [53].

It is suggested that the constant S value in the NM state for Co_2TiSi, Co_2TiGe and Co_2TiSn (**Figure 4(b)**) is governed by the relaxation time rather than by the electronic structure [38]. The S value is calculated by using Eq. (1), where both the numerator and denominator of the fraction are functions of relaxation time $\tau(k, T)$; τ is included in both numerator and denominator of the fraction through $\tilde{\boldsymbol{\sigma}}(\varepsilon, T)$ described in Eq. (6). However, in the calculation, the τ in the numerator and denominator cancels each other. In addition, the total S is calculated assuming that τ for the majority and minority spin electrons is the same (Eq. (7)). The neglected τ in Eqs. (1) and (7) could be a reason for the difference in the temperature dependence of the calculated and measured S. Another possible reason for this discrepancy is the method employed in calculating the electronic structure. The calculation results shown in **Figures 3** and **6** are based on the LSDA or PBE-GGA. The use of the onsite Hubbard interaction in combination with PBE-GGA, namely, PBE + U or GGA + U [51, 55, 70, 73], and the Tran-Blaha modified Becke-Johnson (TB-MBJ) [64, 73] gives electronic structures different from that obtained using the LSDA or PBE-GGA, which may lead to a temperature dependence of S well-fitted to the measured one.

Also, defect and/or disorder in full-Heusler compounds affect the temperature dependence, as well as the sign of S, which could be another reason for the

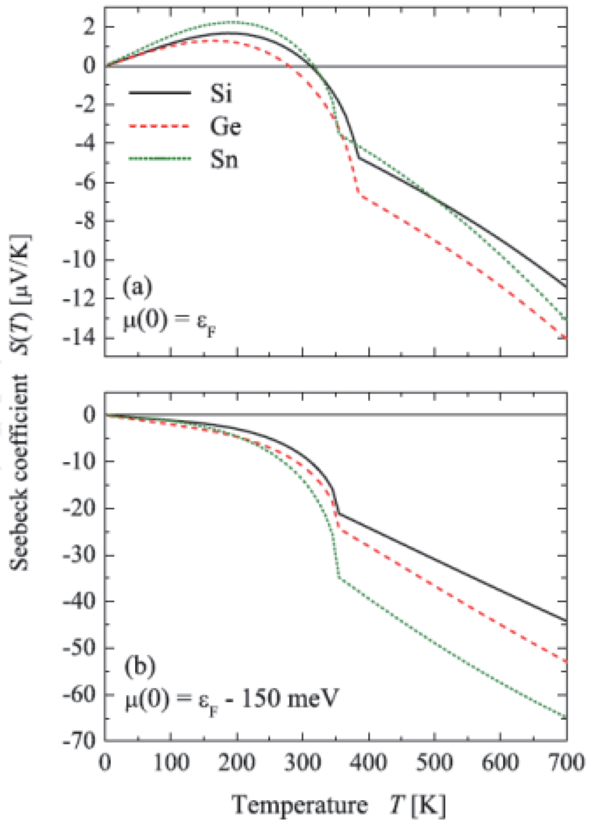

Figure 6.
Temperature dependence of the calculated S *of* Co_2TiZ *(Z = Si, Ge, Sn) considering the FM-NM phase transition. In the calculation, the chemical potential at* T = 0, μ(0), *was set to (a)* ε_F *and (b) 150 meV below* ε_F*. (Reprinted from [38]. Copyright 2010, with permission from American Physical Society).*

discrepancy in the temperature dependence of *S*. The structure model used for the calculation in **Figures 3** and **6** is the $L2_1$, X or Y structure, which is highly ordered phases, devoid of any defect, for the ternary and quaternary full-Heusler compounds. Popescu et al. [52] investigated the effect of several defects on the temperature dependence of *S* for Co_2TiZ (*Z* = Si, Ge, Sn) in the FM state. As shown in **Figure 7**, off-stoichiometric defects, such as Co vacancy and the substitution of excess atoms at a particular site, change the sign of *S*.

The effect of structural disorder on *S* for Co_2CrAl, Co_2MnAl, Co_2MnSi, Co_2FeAl and Co_2FeSi has been obtained, as shown in **Figure 8** [53]. The figure compares the calculated $S_{FM + NM}$ with the measured *S*. It is observed that the measured values of *S* are individually higher than the calculated value ($S_{FM + NM}$). Considering the crystal structure, Co_2CrAl, Co_2MnAl, Co_2MnSi, Co_2FeAl and Co_2FeSi are not in the fully ordered $L2_1$ structure; most of them crystallise in the disordered B2 and/or A2 structures. This result implies that the B2 and/or A2 structures exhibit higher *S* than the $L2_1$ structure. Recently, Li et al. [78] investigated the effect of structural disorder on the value of *S* for half-metallic Mn_2VAl compounds by varying the B2 order degree. **Figure 9(a)** shows the measured *S* values for Mn_2VAl with the B2 order degree of 27 and 66%. The *S* values for the structure having 66% B2 order degree are observed to be higher than those for 27% B2 order degree in the entire measurement temperature range. In addition, it is observed that the *S* value increases with increasing the B2 order degree (**Figure 9(b)**). The increase in the B2 order degree means an increase in the disorder between the V and Al atoms, that is, a decrease in the $L2_1$ order degree. To understand the reason for the difference in *S* between the $L2_1$ and B2 structures, the DOS of Mn_2VAl with the $L2_1$ and B2 structures was calculated by using the Korringa-Kohn-Rostoker method. It was obtained that the B2 structure exhibits a steeper DOS of the majority-spin *sp*-electrons than the $L2_1$

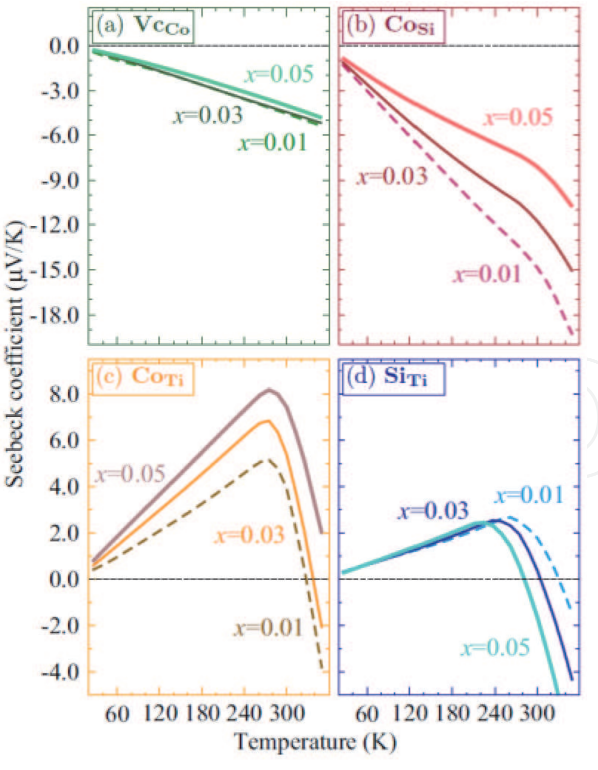

Figure 7.
Change in calculated S for Co_2TiSi with several off-stoichiometric defects such as (a) Co vacancy (V_{Co}), (b) excess Co atoms at the Si site (Co_{Si}), (c) excess Co atoms at the Ti site (Co_{Ti}) and (d) excess Si atoms at the Ti site (Si_{Ti}). (Reprinted from [52]. Copyright 2017, with permission from American Physical Society).

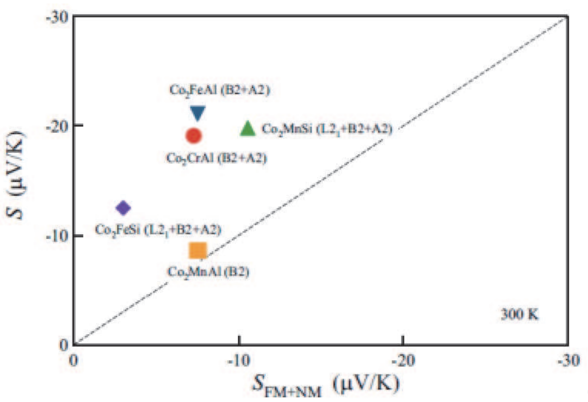

Figure 8.
Comparison between the calculated S_{FM+NM} and the measured S at 300 K for several Co-based full-Heusler compounds. (Reprinted from [53]. Copyright 2017, with permission from Springer).

structure, which is considered as the main reason for the higher *S* of the B2 structure than that of the $L2_1$ structure. Further increase in the B2 order degree is expected to yield a higher *S* for Mn_2VAl. The modulation of the order degree can be a key strategy to enhance the *S* value of the half-metallic full-Heusler compounds; the disorder in Co_2CrAl, Co_2MnAl, Co_2MnSi, Co_2FeAl, Co_2FeSi and Mn_2VAl gives rise to the higher *S*. To establish this strategy, the effects of the order degree, not only on *S* but also on σ, should be investigated for several half-metallic full-Heusler compounds.

Considering the TE performance of the half-metallic full-Heusler compounds, not only PF but also zT are important. To evaluate the zT of Co_2MnSi, we obtained the temperature dependence of the total thermal conductivity, κ_{tot} (**Figure 10(a)**). Similar to the case of common metals, a high κ_{tot} was obtained. It decreases with increasing temperature from 79 W/Km at 300 K to 21 W/Km at 1000 K.

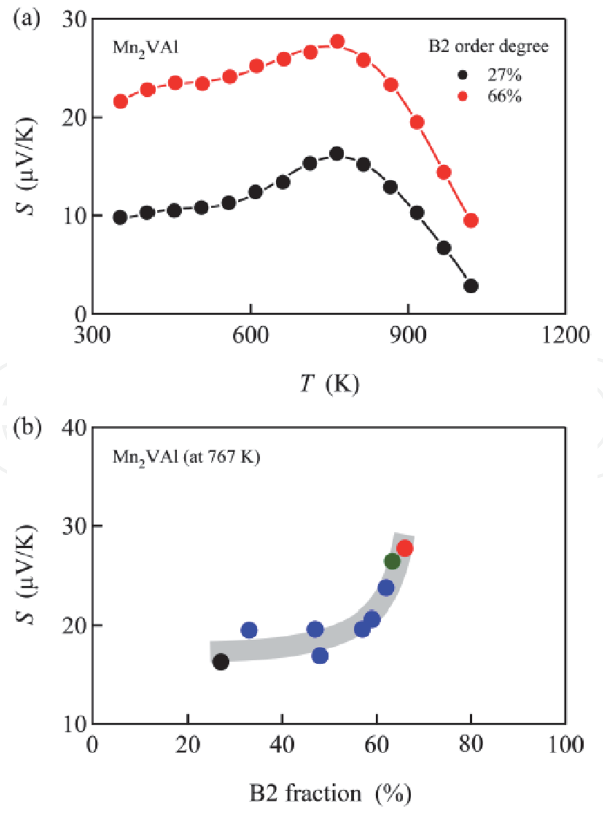

Figure 9.
(a) Temperature dependence of the measured S of Mn_2VAl with the B2 order degree of 27 and 66%. (b) Measured S values of Mn_2VAl at 767 K plotted against the B2 order degree. (Reprinted from [78]. Copyright 2020, with permission from IOP Publishing).

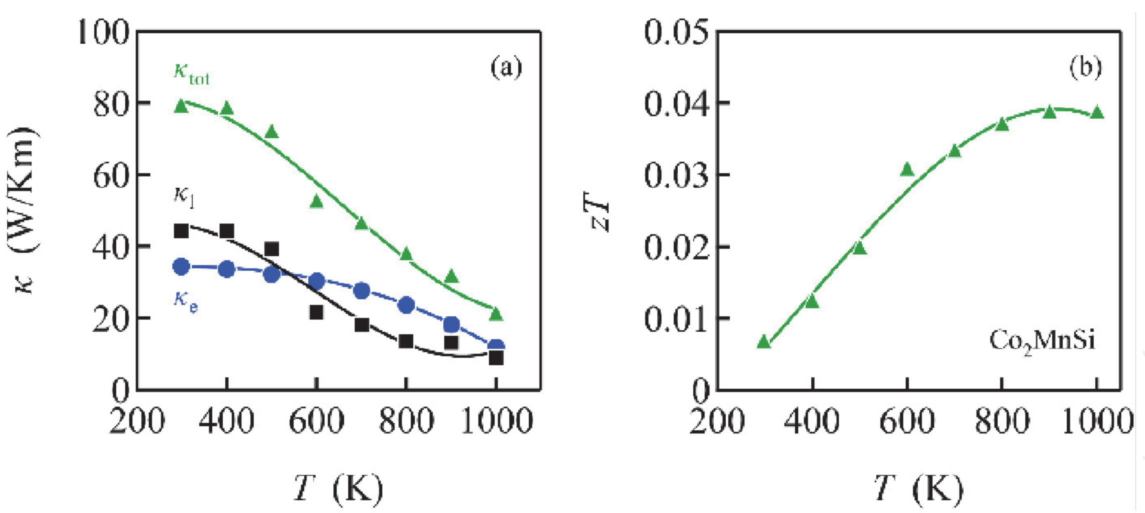

Figure 10.
Temperature dependence of (a) measured κ_{tot}, κ_e and κ_l and (b) evaluated zT of Co_2MnSi.

Figure 10(b) shows the temperature dependence of zT for Co_2MnSi calculated using the PF value (**Figure 5(b)**) and the κ_{tot} value (**Figure 10(a)**). Due to the high κ_{tot}, the maximum zT value, zT_{max}, of Co_2MnSi is 0.039, which is obtained at temperatures above 900 K. Although this zT_{max} value is far below the standard level of zT = 1, it is higher than that of Co_2TiSn (0.033 at 370–400 K) [38] and those of semi-metallic full-Heusler compounds (0.0052 at 300 K for Ru_2NbAl [28] and 0.0027 at 300 K for $Ru_2VAl_{0.25}Ga_{0.75}$ [29]).

It should be noted that the κ_{tot} of Co_2MnSi is not equal to the carrier thermal conductivity, κ_e. The κ_e value can be calculated by using the Wiedemann-Frantz law, $\kappa_e = L\sigma T$, where L is the Lorentz number. Evaluating the L value on the basis of the single parabolic band model [87] and using the measured σ value (**Figure 5(a)**), the κ_e value of Co_2MnSi was calculated and plotted in **Figure 10(a)**. It can be observed from the figure that κ_e is only half as high as κ_{tot}. The rest is attributed to the lattice thermal conductivity, κ_l (=$\kappa_{tot} - \kappa_e$), as shown in **Figure 10(a)**, which amounts to a half of the κ_{tot}. This is contrary to the case of common metals where the κ_{tot} is mainly dominated by κ_e [88]. The non-negligible κ_l suggests that, for the theoretical evaluation of zT of the half-metallic full-Heusler compounds, the contribution of κ_l should not be ignored. Experimentally, the high contribution of κ_l to κ_{tot} indicates that the κ_{tot} of half-metallic full-Heusler compounds could be reduced by decreasing the κ_l.

4. Future prospects of magnetic full-Heusler compounds as potential thermoelectric materials

In this section, we introduce other full-Heusler compounds to demonstrate the potentials of magnetic full-Heusler compounds in TE applications. First, we consider the full-Heusler SGSs as an example. Schematic illustrations of the DOS of SGSs and HMs are shown in **Figure 11**. The DOS of SGSs has an open band gap in one spin electron and a closed gap in the other. Since the Fermi level ε_F is located just at the closed gap, the electron or hole concentration in SGSs is expected to be less than that in HMs. One of the investigated SGSs is the full-Heusler Mn_2CoAl, which crystallises in the X structure (the inverse Heusler phase). The variation of its σ, S and carrier concentration, n, with temperature is shown in **Figure 12**, as determined by Ouardi et al. [19]. It can be observed that the σ and n vary slightly with the temperature, which is attributed to the typical behaviour of gapless semiconductors [89]. In addition, the S value is nearly equal to 0 μV/K. The reduced Seebeck effect indicates the occurrence of electron and hole compensation, which is the evidence that ε_F is at the top of the valence states and at the bottom of the conduction states.

Owing to the nearly zero S values, Mn_2CoAl cannot be used as a TE material; however, there is a possibility of achieving high $|S|$ in Mn_2CoAl by tuning the position of ε_F. The position of ε_F can be varied via partial substitution, which increases the hole or electron carrier concentration in Mn_2CoAl. We calculated the S value for the partially substituted Mn_2CoAl, as shown in **Figure 13(a)**. The calculation was based on a rigid band model; thus, the electronic structure of the partially substituted Mn_2CoAl is assumed to be the same as that of Mn_2CoAl. In the figure, the horizontal axis is μ-ε_F, where μ and ε_F are the chemical potential (i.e., the Fermi

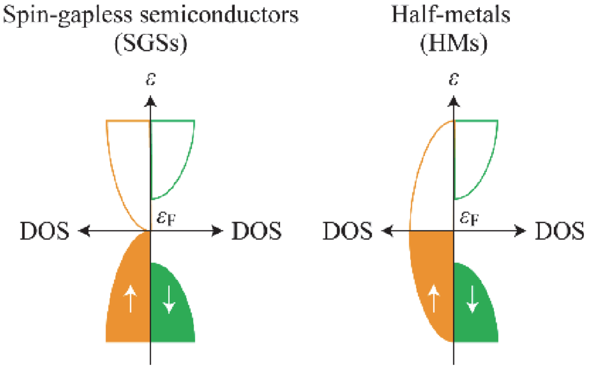

Figure 11.
Schematic illustration of DOS for spin-gapless semiconductors (SGSs) and half-metals (HMs).

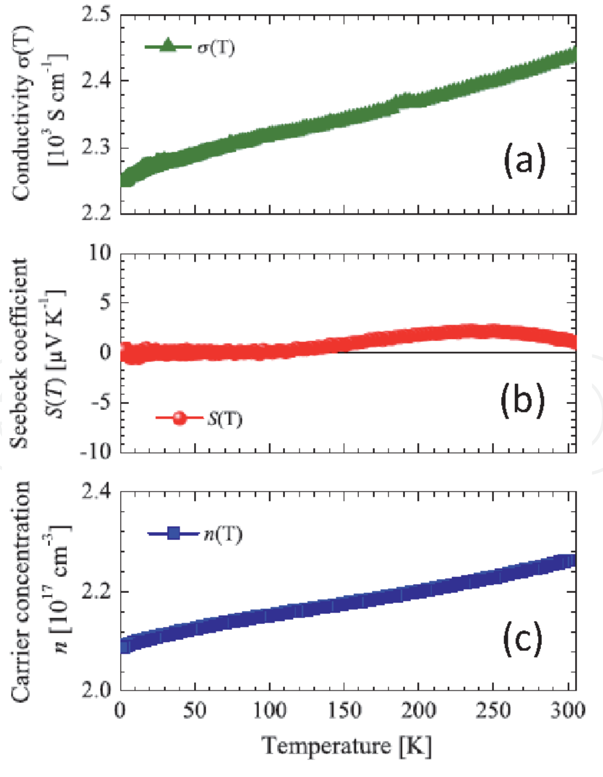

Figure 12.
Temperature dependence of the measured (a) σ, (b) S and (c) n of Mn_2CoAl. (Reprinted from [19]. Copyright 2020, with permission from American Physical Society).

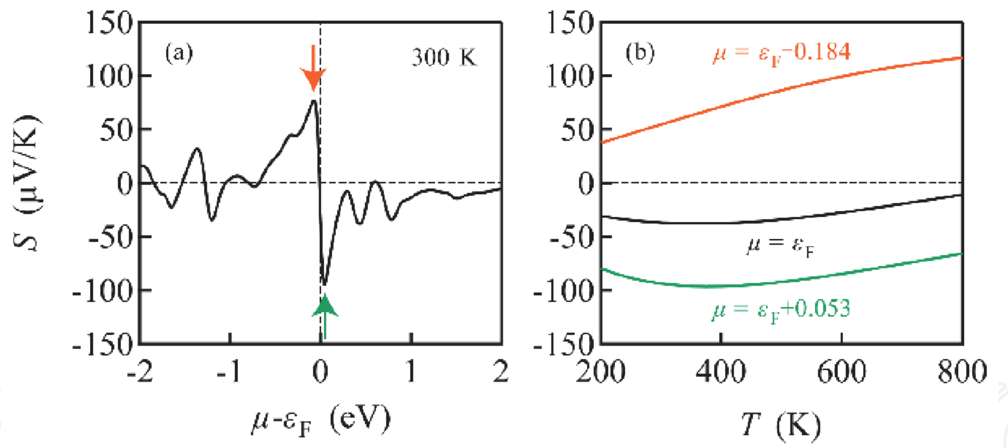

Figure 13.
(a) Calculated S value at 300 K for the partially substituted Mn_2CoAl plotted as a function of μ-ε_F, where μ and ε_F are the Fermi levels of partially substituted Mn_2CoAl and that of Mn_2CoAl, respectively. The highest |S| values are obtained at $\mu = \varepsilon_F - 0.184$ and at $\mu = \varepsilon_F + 0.053$, as denoted by orange and green arrows, respectively. (b) Temperature dependence of S at $\mu = \varepsilon_F$, $\mu = \varepsilon_F - 0.184$ and $\mu = \varepsilon_F + 0.053$.

level) of the partially substituted Mn_2CoAl and the Fermi level of Mn_2CoAl, respectively. A negative/positive μ-ε_F value means an increase in the hole/electron carrier concentration. Although the value of S at $\mu = \varepsilon_F$, corresponding to the case of Mn_2CoAl, is small, it is large at $\mu = \varepsilon_F - 0.184$ and at $\mu = \varepsilon_F + 0.053$ (pointed by orange and green arrows, respectively). The temperature dependences of S at $\mu = \varepsilon_F$, $\mu = \varepsilon_F - 0.184$ and $\mu = \varepsilon_F + 0.053$ are shown in **Figure 13(b)**, which again demonstrates that high $|S|$ values can be achieved for both p-type and n-type regions. These calculation results prove the full-Heusler SGSs as potential materials for TE applications.

To achieve high $|S|$ values for Mn_2CoAl, it is important to retain its SGS characteristic. Galanakis et al. [90] theoretically investigated the effects of structural disorder on the electronic structure of Mn_2CoAl. It was obtained that the SGS characteristic is not conserved in the presence of Mn-Co, Mn-Al and Co-Al antisite defects. Instead of the closed gap, low DOS intensity emerges in the electronic structure of the majority spin electrons around ε_F, indicating that the disorder induces half-metallic characteristics in Mn_2CoAl. Also, Xu et al. [91] reported that an as-prepared Mn_2CoAl compound is non-stoichiometric and contains the Mn-Co antisite defect. In a case where Mn_2CoAl is not an SGS, the $|S|$ cannot be increased via partial substitutions.

Other examples considered here are the full-Heusler compounds having low values of κ_l. **Figure 14** shows a flower-like microstructure of $Co_2Dy_{0.5}Mn_{0.5}Sn$ observed by Schwall et al. [43]. Although the chemical composition of $Co_2Dy_{0.5}Mn_{0.5}Sn$ coincides with that of the full-Heusler phase, $Co_2Dy_{0.5}Mn_{0.5}Sn$ is not in a single phase. It consists of two major phases: half-metallic Co_2MnSn and ferromagnetic $Co_8Dy_3Sn_4$ phases. This phase separation is induced by rapid cooling from the liquid phase. Consequently, the κ_l value of $Co_2Dy_{0.5}Mn_{0.5}Sn$ is lower than those of Co_2MnSn and $Co_8Dy_3Sn_4$.

He et al. [9] theoretically discovered a new class of stable nonmagnetic full-Heusler semiconductors with high PF and ultralow κ_l, attributed to atomic rattling. The compounds contain alkaline earth elements (Ba, Sr or Ca) in the X sublattice and noble metals (Au or Hg) and main group elements (Sn, Pb, As or Sb) in the Y and Z sublattices, respectively. The κ_l value of Ba_2AuBi and Ba_2HgPb was obtained to be lower than 0.5 W/Km at 300 K. At higher temperatures, it was close to the theoretical minimum, that is, the amorphous limit of 0.27 W/Km [92]. Park et al. [16] further examined the TE properties of Ba_2BiAu. They predicted that considerably high zT of ~5 can be achieved at 800 K.

Finally, there are many ternary and quaternary full-Heusler compounds yet to be explored. Among the full-Heusler compounds, nonmagnetic Fe_2VAl-based compounds have been intensively investigated as one of the potential TE semiconductors [93]. Despite the long historical investigation, Hinterleitner et al. [94] discovered quite recently that a metastable $Fe_2V_{0.8}W_{0.2}Al$ thin film exhibits extremely high zT of ~6 at 350 K as a result of its high S. The crystal structure of the thin film is reported to be the disordered A2 structure, which could be the reason for its high S, as in the cases of several half-metallic Co-based and Mn-based full-Heusler compounds [53, 78]. If the disorder in structure contributes to the high S, then the strategy of enhancing zT by controlling structural disorder would be applicable to the other full-Heusler compounds. Herewith, more conventional and novel findings on the full-Heusler compounds can be achieved.

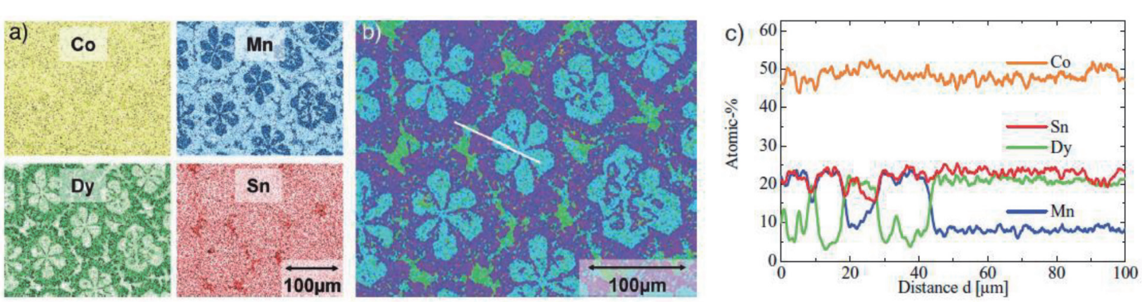

Figure 14.
Flower-like microstructure of $Co_2Dy_{0.5}Mn_{0.5}Sn$. (a) Elemental mappings, (b) combined image of elemental mappings shown in (a). (c) Line scan along the line indicated in (b). (Reprinted from [43]. Copyright 2012, with permission from WILEY-VCH).

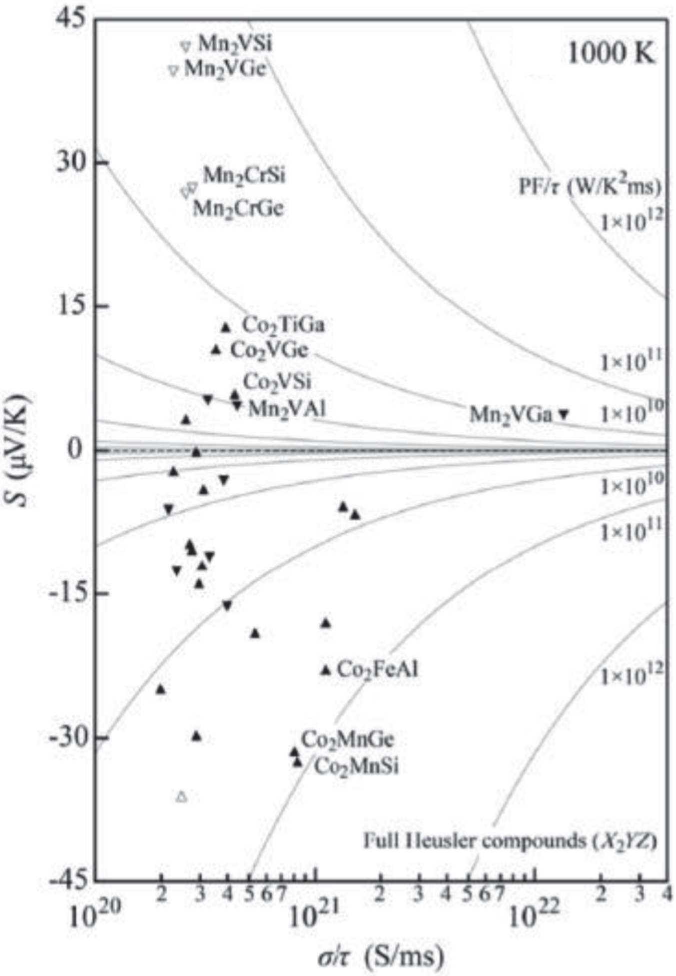

Figure 15.
Calculated S *versus* σ/τ *at 1000 K for several Co-based and Mn-based full-Heusler compounds. The grey curves indicate PF/*τ*. (Reprinted from [60]. Copyright 2018, with permission from Elsevier).*

To explore the potentials of the full-Heusler compounds, theoretical studies are vital to minimise the experimental tasks. **Figure 15** exhibits a plot of S versus σ/τ at 1000 K for several Co-based and Mn-based full-Heusler compounds, as calculated by Li et al. [60]. Furthermore, recent advancements in machine learning dispel the difficulty in searching novel full-Heusler compounds [95, 96]. Combining such calculations with experiments, we can effectively discover magnetic full-Heusler compounds with much higher TE efficiency, which promises the realisation of high-efficiency TE power generation devices.

Acknowledgements

We greatly acknowledge the financial supports from the Thermal and Electric Energy Technology Foundation and from the Tsinghua-Tohoku Collaborative Research Fund.

Conflict of interest

We declare that there is no conflict of interest.

Nomenclatures

η_{max} [−]	maximum TE efficiency
zT [−]	dimensionless figure-of-merit
T [K]	absolute temperature
S [V/K]	Seebeck coefficient
σ [S/m]	electrical conductivity
κ [W/Km]	thermal conductivity
PF [W/K^{2}m]	power factor
ε_i [eV]	electronic energy–wavenumber dispersion curve of the i-th band
$\boldsymbol{k}$ [m^{-1}]	wavenumber
$\boldsymbol{S}$ [V/K]	Seebeck coefficient tensor
$\boldsymbol{\sigma}$ [S/m]	electrical conductivity tensor
$\boldsymbol{\kappa}_{\mathrm{e}}$ [W/Km]	carrier thermal conductivity tensor
$e = 1.60217662 \times 10^{-19}$ C	elementary charge
ε [eV]	electron energy
ε_{F} [eV]	Fermi level
f_{FD} [−]	Fermi-Dirac distribution function
N_k [−]	total number of k-points
τ [1/s]	relaxation time
$= 6.582119569 \times 10^{-16}$ eVs	Dirac constant
$\tilde{\boldsymbol{\sigma}}$ [S/m]	conductance spectrum tensor
DOS [states/eV]	density of states
M [−]	normalised magnetisation calculated by using molecular field theory
μ [eV]	chemical potential
κ_{e} [W/Km]	carrier thermal conductivity
L [WΩ/K^2]	Lorentz number
κ_{l} [W/Km]	lattice thermal conductivity
n [1/m^3]	carrier concentration

Author details

Kei Hayashi*, Hezhang Li, Mao Eguchi, Yoshimi Nagashima and Yuzuru Miyazaki
Department of Applied Physics, Graduate School of Engineering, Tohoku University, Sendai, Japan

*Address all correspondence to: hayashik@crystal.apph.tohoku.ac.jp

References

[1] Rowe DM, editor. Thermoelectrics Handbook: Macro to Nano. Boca Raton, FL: CRC Press; 2005. p. 1022

[2] Uher C. Materials Aspect of Thermoelectricity. Boca Raton, FL: CRC Press; 2016. p. 610

[3] Kurosaki K, Takagiwa Y, Shi X, editors. Thermoelectric Materials: Principles and Concepts for Enhanced Properties. Berlin: De Gruyter; 2020. p. 280

[4] Heusler F, Starck W, Haupt E. Magnetisch-chemische Studien. Verhandlungen der Deutschen Physikalischen Gesellschaft. 1903;**5**: 219-232 (in German)

[5] Webster P. Heusler alloys. Contemporary Physics. 1969;**10**:559-577. DOI: 10.1080/00107516908204800

[6] Webster PJ, Ziebeck KRA. Heusler alloys. In: Wijn HRJ, editor. Landolt-Börnstein New Series Group III. Vol. 19C. Berlin: Springer; 1988. pp. 75-185

[7] Kübler J, William AR, Sommers CB. Formation and coupling of magnetic moments in Heusler alloys. Physical Review B. 1983;**28**:1745-1755. DOI: 10.1103/PhysRevB.28.1745

[8] Ishida S, Fujii S, Kashiwagi S, Asano S. Search for half-metallic compounds in Co_2MnZ (Z=IIIb, IVb, Vb element). Journal of the Physical Society of Japan. 1995;**64**:2152-2157. DOI: 10.1143/JPSJ.64.2152

[9] He J, Amsler M, Xia Y, Naghavi SS, Hegde VI, Hao S, et al. Ultralow thermal conductivity in full Heusler semiconductors. Physical Review Letters. 2016;**117**:046602. DOI: 10.1103/PhysRevLett.117.046602

[10] Li J, Li J, Zhang Q, Zhang Z, Yang G, Ma H, et al. The thermoelectric properties of predicted semiconducting Ti_2CrGe and Ti_2CrSn: A first principles study. Computational Materials Science. 2016;**125**:183-187. DOI: 10.1016/j.commatsci.2016.08.048

[11] Li J, Yang G, Yang Y, Ma H, Zhang Q, Zhang Z, et al. Electronic and thermoelectric properties of nonmagnetic inverse Heusler semiconductors Sc_2FeSi and Sc_2FeGe. Journal of Magnetism and Magnetic Materials. 2017;**442**:371-376. DOI: 10.1016/j.jmmm.2017.07.010

[12] Yousuf S, Gupta DC. Insight into electronic, mechanical and transport properties of quaternary CoVTiAl: Spin-polarized DFT + U approach. Materials Science and Engineering B. 2017;**221**: 73-79. DOI: 10.1016/j.mseb.2017.04.004

[13] Zhang Q, Ma H, Yang G, Yang Y, Li J, Li C, et al. Prediction of fully compensated ferrimagnetic and nonmagnetic semiconductors with promising thermoelectric properties through the Mo substitution of Cr for Ti_2CrZ (Z=Ge, Sn) Heusler alloys. Intermetallics. 2018;**96**:72-78. DOI: 10.1016/j.intermet.2018.03.001

[14] Yan Y, Yang J, Li J, Wang Y, Ren W. High thermoelectric properties in full-Heusler X_2YZ alloys (X = Ca, Sr, and Ba; Y = Au and Hg; Z = Sn, Pb, As, Sb, and Bi). Journal of Physics D: Applied Physics. 2019;**52**:495303. DOI: 10.1088/1361-6463/ab40e6

[15] Matougui M, Bouadjemi B, Houari M, Haid S, Lantri T, Zitouni A, et al. Rattling Heusler semiconductors' thermoelectric properties: First-principles prediction. Chinese Journal of Physics. 2019;**57**:195-210. DOI: 10.1016/j.cjph.2018.11.015

[16] Park J, Xia Y, Ozoliņš V. High thermoelectric power factor and efficiency from a highly dispersive band in Ba_2BiAu. Physical Review Applied.

2019;**11**:014058. DOI: 10.1103/PhysRevApplied.11.014058

[17] Lin TT, Gao Q, Liu GD, Dai XF, Zhang XM, Zhang HB. Dynamical stability, electronic and thermoelectric properties of quaternary ZnFeTiSi Heusler compound. Current Applied Physics. 2019;**19**:721-727. DOI: 10.1016/j.cap.2019.03.020

[18] Enamullah Cha P-R. The n- and p-type thermoelectric response of a semiconducting Co-based quaternary Heusler alloy: A density functional approach. Journal of Materials Chemistry C. 2019;**7**:7664-7671. DOI: 10.1039/c9tc00570f

[19] Ouardi S, Fecher GH, Felser C, Kübler J. Realization of spin gapless semiconductors: The Heusler compound Mn_2CoAl. Physical Review Letters. 2013;**110**:100401. DOI: 10.1103/PhysRevLett.110.100401

[20] Yousuf S, Gupta DC. Thermoelectric and mechanical properties of gapless Zr_2MnAl compound. Indian Journal of Physics. 2017;**91**:33-41. DOI: 10.1007/s12648-016-0900-3

[21] Patel PD, Shinde S, Gupta SD, Dabhi SD, Jha PK. The first principle calculation of structural, electronic, magnetic, elastic, thermal and lattice dynamical properties of fully compensated ferrimagnetic spin-gapless heusler alloy Zr_2MnGa. Computational Condensed Matter. 2018;**15**:61-68. DOI: 10.1016/j.cocom.2018.02.003

[22] Chen X, Huang Y, Yuan H, Liu J, Chen H. Theoretical investigation on thermoelectric properties of spin gapless semiconductor Cr_2ZnSi. Applied Physics A: Materials Science & Processing. 2018;**124**:841. DOI: 10.1007/s00339-018-2259-0

[23] Rani D, Enamullah, Bainsla L, Suresh KG, Alam A. Spin-gapless semiconducting nature of Co-rich $Co_{1+x}Fe_{1-x}CrGa$. Physical Review B. 2019;**99**:104429. DOI: 10.1103/PhysRevB.99.104429

[24] Yousuf S, Hien ND, Batoo KM, Raslan EH, Gupta DC. Insight into structural, electronic and thermoelectric properties of Zr_2MnX (X=Ga, In) Heuslers. Materials Research Express. 2019;**6**:046530. DOI: 10.1088/2053-1591/aafb1d

[25] Patel PD, Shinde SM, Gupta SD, Jha PK. A promising thermoelectric response of fully compensated ferrimagnetic spin gapless semiconducting Heusler alloy Zr_2MnAl at high temperature: DFT study. Materials Research Express. 2019;**6**:076307. DOI: 10.1088/2053-1591/ab1723

[26] Patel PD, Shinde S, Gupta SD, Jha PK. Investigation of structural and elastic stability, electronic, magnetic, thermoelectric, lattice-dynamical and thermodynamical properties of spin gapless semiconducting Heusler alloy Zr_2MnIn using DFT approach. Journal of Electronic Materials. 2019;**48**:1634-1642. DOI: 10.1007/s11664-018-06911-y

[27] Kuo CN, Lee HW, Wei C-M, Lin YH, Kuo YK, Lue CS. Ru_2NbGa: A Heusler-type compound with semimetallic characteristics. Physical Review B. 2016;**94**:205116. DOI: 10.1103/PhysRevB.94.205116

[28] Mondal S, Mazumdar C, Ranganathan R, Alleno E, Sreeparvathy PC, Kanchana V, et al. Ferromagnetically correlated clusters in semimetallic Ru_2NbAl Heusler alloy and its thermoelectric properties. Physical Review B. 2018;**98**:205130. DOI: 10.1103/PhysRevB.98.205130

[29] Ramachandran B, Lin YH, Kuo YK, Kuo CN, Gippius AA, Lue CS. Thermoelectric properties of Heusler-type $Ru_2VAl_{1-x}Ga_x$ alloys.

Intermetallics. 2018;**92**:36-41. DOI: 10.1016/j.intermet.2017.09.012

[30] Fichtner T, Kreiner G, Chadov S, Fecher GH, Schnelle W, Hoser A, et al. Magnetic and transport properties in the Heusler series $Ni_{2-x}Mn_{1+x}Sn$ affected by chemical disorder. Intermetallics. 2015; **57**:101-112. DOI: 10.1016/j.intermet. 2014.10.012

[31] Khandy SA, Islam I, Gupta DC, Laref A. Predicting the electronic structure, magnetism, and transport properties of new Co-based Heusler alloys. International Journal of Energy Research. 2018;**42**:4221-4228. DOI: 10.1002/er.4182

[32] Khelfaoui F, Boudali A, Bentayeb A, El Hachemi OL, Si AY. Investigations of structural, elastic, electronic, magnetic and transport properties of the heusler compounds Zr_2PdZ (Z = Al, Ga, and In): FP-LAPW method. Acta Physica Polonica A. 2018;**133**:157-163. DOI: 10.12693/APhysPolA.133.157

[33] Benzoudji F, Bensaid D, el Kader YA, Arbouche O, Bouyakoub AZ, Moulay N, et al. The preference of the ferromagnetic ordering for the novel Heusler Rh_2MnTi compound. Journal of Superconductivity and Novel Magnetism. 2019;**32**: 1415-1421. DOI: 10.1007/s10948-018-4837-y

[34] Duan J, Yin-Wei W, A-Peng Z, Liu S, Dar SA. Electronic structure, elastic, mechanical, thermodynamic and thermoelectric investigations of Mn_2PtX (X=Rh, Pd) Heusler alloys. Solid State Communications. 2019;**290**:12-21. DOI: 10.1016/j.ssc.2018.12.013

[35] Galanakis I, Özdoğan K, Şaşıoğlu E, Aktaş B. Ab initio design of half-metallic fully compensated ferrimagnets: The case of Cr_2MnZ (Z=P, As, Sb, and Bi). Physical Review B. 2007;**75**:172405. DOI: 10.1103/PhysRevB.75.172405

[36] Graf T, Fecher GH, Barth J, Winterlik J, Felser C. Electronic structure and transport properties of the Heusler compound Co_2TiAl. Journal of Physics D: Applied Physics. 2009;**42**: 084003. DOI: 10.1088/0022-3727/42/8/084003

[37] Balke B, Ouardi S, Graf T, Barth J, Blum CGF, Fecher GH, et al. Seebeck coefficients of half-metallic ferromagnets. Solid State Communications. 2010;**150**:529-532. DOI: 10.1016/j.ssc.2009.10.044

[38] Barth J, Fecher GH, Balke B, Ouardi S, Graf T, Felser C, et al. Itinerant half-metallic ferromagnets Co_2TiZ (Z=Si, Ge, Sn): Ab initio calculations and measurement of the electronic structure and transport properties. Physical Review B. 2010;**81**: 064404. DOI: 10.1103/PhysRevB.81.064404

[39] Sharma V, Solanki AK, Kashyap A. Electronic, magnetic and transport properties of Co_2TiZ (Z=Si, Ge and Sn): A first-principle study. Journal of Magnetism and Magnetic Materials. 2010;**322**:2922-2928. DOI: 10.1016/j.jmmm.2010.05.006

[40] Graf T, Barth J, Balke B, Populoh S, Weidenkaff A, Felser C. Tuning the carrier concentration for thermoelectrical application in the quaternary Heusler compound $Co_2TiAl_{1-x}Si_x$. Scripta Materialia. 2010; **63**:925-928. DOI: 10.1016/j.scriptamat.2010.07.001

[41] Graf T, Barth J, Blum CGF, Balke B, Felser C. Phase-separation-induced changes in the magnetic and transport properties of the quaternary Heusler alloy $Co_2Mn_{1-x}Ti_xSn$. Physical Review B. 2010;**82**:104420. DOI: 10.1103/PhysRevB.82.104420

[42] Barth J, Fecher GH, Balke B, Graf T, Shkabko A, Weidenkaff A, et al. Anomalous transport properties of the

half-metallic ferromagnets Co_2TiSi, Co_2TiGe and Co_2TiSn. Philosophical Transactions of the Royal Society A. 2011;**369**:3588-3601. DOI: 10.1098/rsta.2011.0183

[43] Schwall M, Schoop LM, Ouardi S, Balke B, Felser C, Klaer P, et al. Thermomagnetic properties improved by self-organized flower-like phase separation of ferromagnetic $Co_2Dy_{0.5}Mn_{0.5}Sn$. Advanced Functional Materials. 2012;**22**:1822-1826. DOI: 10.1002/adfm.201102792

[44] Sharma S, Pandey SK. Investigation of thermoelectric properties of half-metallic Co_2MnGe by using first principles calculations. Journal of Physics: Condensed Matter. 2014;**26**:215501. DOI: 10.1088/0953-8984/26/21/215501

[45] Mohankumar R, Ramasubramanian S, Rajagopalan M, Manivel Raja M, Kamat SV, Kumar J. Effect of Fe substitution on the electronic structure, magnetic and thermoelectric properties of Co_2FeSi full Heusler alloy: A first principle study. Computational Materials Science. 2015;**109**:34-40. DOI: 10.1016/j.commatsci.2015.07.001

[46] Sharma S, Pandey SK. Applicability of two-current model in understanding the electronic transport behavior of inverse Heusler alloy: Fe_2CoSi. Physics Letters A. 2015;**379**:2357-2361. DOI: 10.1016/j.physleta.2015.04.019

[47] Bhat IH, Yousuf S, Mohiuddin Bhat T, Gupta DC. Investigation of electronic structure, magnetic and transport properties of half-metallic Mn_2CuSi and Mn_2ZnSi Heusler alloys. Journal of Magnetism and Magnetic Materials. 2015;**395**:81-88. DOI: 10.1016/j.jmmm.2015.07.022

[48] Bhat TM, Gupta DC. Transport, structural and mechanical properties of quaternary FeVTiAl alloy. Journal of Electronic Materials. 2016;**45**:6012-6018. DOI: 10.1007/s11664-016-4827-4

[49] Yalcin BG. Ground state properties and thermoelectric behavior of Ru_2VZ (Z=Si, Ge, Sn) half-metallic ferromagnetic full-Heusler compounds. Journal of Magnetism and Magnetic Materials. 2016;**408**:137-146. DOI: 10.1016/j.jmmm.2016.02.064

[50] Reshak AH. Transport properties of Co-based Heusler compounds Co_2VAl and Co_2VGa: Spin-polarized DFT+U. RSC Advances. 2016;**6**:54001-54012. DOI: 10.1039/c6ra10226c

[51] Bhat TM, Gupta DC. Robust thermoelectric performance and high spin polarisation in CoMnTiAl and FeMnTiAl compounds. RSC Advances. 2016;**6**:80302. DOI: 10.1039/C6RA18934B

[52] Popescu V, Kratzer P, Wimmer S, Ebert H. Native defects in the Co_2TiZ (Z=Si,Ge,Sn) full Heusler alloys: Formation and influence on the thermoelectric properties. Physical Review B. 2017;**96**:054443. DOI: 10.1103/PhysRevB.96.054443

[53] Hayashi K, Eguchi M, Miyazaki Y. Structural and thermoelectric properties of ternary full-Heusler alloys. Journal of Electronic Materials. 2017;**46**:2710-2716. DOI: 10.1007/s11664-016-4944-0

[54] Yousuf S, Gupta DC. Insight into mechanical properties and thermoelectric efficiency of Zr_2CoZ (Z = Si, Ge) Heusler alloys. Materials Research Express. 2017;**4**(11):6307. DOI: 10.1088/2053-1591/aa96cb

[55] Bhat TM, Gupta DC. Effect of on-site coulomb interaction on electronic and transport properties of 100% spin polarized CoMnVAs. Journal of Magnetism and Magnetic Materials. 2017;**435**:173-178. DOI: 10.1016/j.jmmm.2017.04.012

[56] Yousuf S, Khandy SA, Bhat TM, Gupta DC. Evaluation of mechanical and transport properties of Zr_2CoSi Heusler alloy. AIP Conf. Proc. 2017; **1832**:110005. DOI: 10.1063/1.4980629

[57] Yousuf S, Gupta DC. Investigation of electronic, magnetic and thermoelectric properties of Zr_2NiZ (Z = Al,Ga) ferromagnets. Materials Chemistry and Physics. 2017;**192**:33-40. DOI: 10.1016/j.matchemphys.2017.01.056

[58] Patel PD, Pillai SB, Shinde SM, Gupta SD, Jha PK. Electronic, magnetic, thermoelectric and lattice dynamical properties of full heusler alloy Mn_2RhSi: DFT study. Physica B: Condensed Matter. 2018;**550**:376-382. DOI: 10.1016/j.physb.2018.09.020

[59] Gupta DC, Ghosh S. High-pressure and temperature dependence of electronic, magnetic, elastic, thermodynamic, and transport properties of full-Heusler alloys Co_2YIn (Y = Nb, Zr). Journal of Superconductivity and Novel Magnetism. 2018;**31**:2465-2483. DOI: 10.1007/s10948-017-4498-2

[60] Li H, Hayashi K, Miyazaki Y. Design and fabrication of full-Heusler compound with positive Seebeck coefficient as a potential thermoelectric material. Scripta Materialia. 2018;**150**: 130-133. DOI: 10.1016/j.scriptamat.2018.03.018

[61] Yousuf S, Gupta DC. Chemical potential evaluation of thermoelectric and mechanical properties of Zr_2CoZ (Z = Si, Ge) Heusler alloys. Journal of Electronic Materials. 2018;**47**: 2468-2478. DOI: 10.1007/s11664-017-6034-3

[62] Hossain MA, Rahman MT, Khatun M, Haque E. Structural, elastic, electronic, magnetic and thermoelectric properties of new quaternary Heusler compounds CoZrMnX (X=Al, Ga, Ge, In). Computational Condensed Matter. 2018;**15**:31-41. DOI: 10.1016/j.cocom.2018.03.006

[63] Enamullah, Lee S-C. Robust mechanical stability, electronic structure, magnetism and thermoelectric properties of CoFeMnSb quaternary Heusler alloy: A first principle study. Journal of Alloys and Compounds. 2018;**742**:903-909. DOI: 10.1016/j.jallcom.2018.01.330

[64] Bhat TM, Gupta DC. Magneto-electronic, thermal, and thermoelectric properties of some Co-based quaternary alloys. Journal of Physics and Chemistry of Solids. 2018;**112**:190-199. DOI: 10.1016/j.jpcs.2017.09.023

[65] Sunmonu RS, Akinlami JO, Dare EO, Adebayo GA. Effects of Y atom substitution on the structural, magnetic, electronic, elastic, mechanical, thermodynamic and thermoelectric properties of Co_2YAl (Y = Cr, Mn) full Heusler alloys from first principles investigations. Computational Condensed Matter. 2019;**21**:e00412. DOI: 10.1016/j.cocom.2019.e00412

[66] Agbaoye RO, Adebambo PO, Adetunji BI, Osafile O, Adebayo GA. Thermoelectric properties, optimal doping levels and high figure of merit in cobalt-based half/full Heusler alloys by first-principles calculations. Materials Science and Engineering B. 2019;**248**:114409. DOI: 10.1016/j.mseb.2019.114409

[67] Koshi NA, John R. First principles study on the structural, electronic, magnetic and thermoelectric properties of CoX'NbGa (X' = Cr, Mn, Fe) quaternary Heusler alloys. European Physical Journal B. 2019;**92**:86. DOI: 10.1140/epjb/e2019-90663-3

[68] Boudali A, Mokaddem A, Doumi B, Moujri H. Using the spin–orbit coupling

for studying the structural, elastic, electronic, ferromagnetic, and thermoelectric properties of the Ti_2PdX (X = Al, Ga, and in) full-Heusler alloy compounds. Acta Physica Polonica A. 2019;**135**:409-419. DOI: 10.12693/APhysPolA.135.409

[69] Alrahamneh MJ, Mousa AA, Khalifeh JM. First principles study of the structural, electronic, magnetic and thermoelectric properties of Zr_2RhAl. Physica B: Condensed Matter. 2019;**552**: 227-235. DOI: 10.1016/j.physb.2018.10.018

[70] Singh S, Gupta DC. Electronic structure, mechanical, thermoelectric, optical, and thermodynamic properties of yttrium-based quaternary Heusler alloys. International Journal of Energy Research. 2019;**43**:8633-8648. DOI: 10.1002/er.4860

[71] Singh S, Gupta DC. Lanthanum based quaternary Heusler alloys LaCoCrX (X = Al, Ga): Hunt for half-metallicity and high thermoelectric efficiency. Results in Physics. 2019;**13**: 102300. DOI: 10.1016/j.rinp.2019.102300

[72] Chatterjee S, Das S, Pramanick S, Chatterjee S, Giri S, Banerjee A, et al. Anomalous transport and magnetic behaviours of the quaternary Heusler compounds CoFeTiSn and CoFeVGa. Journal of Magnetism and Magnetic Materials. 2019;**478**:155-160. DOI: 10.1016/j.jmmm.2019.01.100

[73] Khandy SA, Chai J-D. Robust stability, half-metallic ferrimagnetism and thermoelectric properties of new quaternary Heusler material: A first principles approach. Journal of Magnetism and Magnetic Materials. 2020;**502**:166562. DOI: 10.1016/j.jmmm.2020.166562

[74] Hoat DM, Naseri M. Examining the half-metallicity and thermoelectric properties of new equiatomic quaternary Heusler compound CoVRhGe under pressure. Physica B: Condensed Matter. 2020;**583**:412058. DOI: 10.1016/j.physb.2020.412058

[75] Sofi SA, Gupta DC. High pressure-temperature study on thermodynamics, half-metallicity, transport, elastic and structural properties of Co-based Heusler alloys: A first-principles study. Journal of Solid State Chemistry. 2020;**284**:121178. DOI: 10.1016/j.jssc.2020.121178

[76] Sofi SA, Gupta DC. Exploration of electronic structure, mechanical stability, magnetism, and thermophysical properties of L21 structured Co_2XSb (X = Sc and Ti) ferromagnets. International Journal of Energy Research. 2020;**44**:2137-2149. DOI: 10.1002/er.5071

[77] Ilkhani M, Boochani A, Amiri M, Asshabi M, Rai DP. Mechanical stability and thermoelectric properties of the PdZrTiAl quaternary Heusler: A DFT study. Solid State Communications. 2020;**308**:113838. DOI: 10.1016/j.ssc.2020.113838

[78] Li H, Hayashi K, Dong J, Li J-F, Miyazaki Y. Distinct impact of order degree on thermoelectric power factor of p-type full-Heusler Mn_2VAl compounds. Materials Research Express. 2020;**7**:055503. DOI: 10.1088/2053-1591/ab875b

[79] Galanakis I, Dederichs PH, Papanikolaou N. Slater-Pauling behavior and origin of the half-metallicity of the full-Heusler alloys. Physical Review B. 2002;**66**:174429. DOI: 10.1103/PhysRevB.66.174429

[80] Skaftouros S, Özdoğan K, Şaşıoğlu E, Galanakis I. Generalized Slater-Pauling rule for the inverse Heusler compounds. Physical Review B.

2013;**87**:024420. DOI: 10.1103/PhysRevB.87.024420

[81] Özdoğan K, Şaşıoğlu E, Galanakis I. Slater-Pauling behavior in LiMgPdSn-type multifunctional quaternary Heusler materials: Half-metallicity, spin-gapless and magnetic semiconductors. Journal of Applied Physics. 2013;**113**:193903. DOI: 10.1063/1.4805063

[82] Allen PB. Boltzmann theory and resistivity of metals. In: Chelikowsky JR, Louie SG, editors. Quantum Theory of Real Materials. Boston: Kluwer; 1996. pp. 219-250

[83] Ziman JM. Electrons and phonons. In: Oxford Classics Series. Oxford: Clarendon Press; 2001. p. 568

[84] Madsen GKH, Singh DJ. BoltzTraP. A code for calculating band-structure dependent quantities. Computer Physics Communications. 2006;**175**:67-71. DOI: 10.1016/j.cpc.2006.03.007

[85] Mott NF, Davis EA. Electronic Processes in Non-Crystalline Materials. Oxford Classic Texts in the Physical Sciences. Oxford: Oxford University Press; 2012. p. 608

[86] Zhang Y, Jia X, Sun H, Sun B, Liu B, Liu H, et al. Suppressing adverse intrinsic conduction of Bi_2Te_3 thermoelectric bulks by Sb and Cu co-substitutions via HPHT synthesis. RSC Advances. 2016;**6**:7378-7383. DOI: 10.1039/C5RA24236C

[87] May AF, Snyder GJ. Introduction to modeling thermoelectric transport at high temperatures. In: Rowe DM, editor. Thermoelectrics and its Energy Harvesting. London: CRC Press; 2012. p. 1

[88] Tong Z, Li S, Ruan X, Bao H. Comprehensive first-principles analysis of phonon thermal conductivity and electron-phonon coupling in different metals. Physical Review B. 2019;**100**:144306. DOI: 10.1103/PhysRevB.100.144306

[89] Tsidilkovski IM. Electron Spectrum of Gapless Semiconductors. Springer Series in Solid-State Sciences. Vol. 116. New York: Springer Berlin; 1997. p. 249. DOI: 10.1007/978-3-642-60403-4

[90] Galanakis I, Özdoğan K, Şaşıoğlu E, Blügel S. Conditions for spin-gapless semiconducting behavior in Mn_2CoAl inverse Heusler compound. Journal of Applied Physics. 2014;**115**:093908. DOI: 10.1063/1.4867917

[91] Xu XD, Chen ZX, Sakuraba Y, Perumal A, Masuda K, Kumara LSR, et al. Microstructure, magnetic and transport properties of a Mn_2CoAl Heusler compound. Acta Materialia. 2019;**176**:33-42. DOI: 10.1016/j.actamat.2019.06.047

[92] Cahill DG, Pohl RO. Lattice vibrations and heat transport in crystals and glasses. Annual Review of Physical Chemistry. 1988;**39**:93-121. DOI: 10.1146/annurev.pc.39.100188.000521

[93] Bharwdaj A, Jat KS, Patnaik S, Parkhomenko YN, Nishino Y, Khovaylo VV. Current research and future prospective of iron-based Heusler alloys as thermoelectric materials. Nanotechnologies in Russia. 2019;**14**:281-289. DOI: 10.1134/S1995078019040049

[94] Hinterleitner B, Knapp I, Poneder M, Shi Y, Müller H, Eguchi G, et al. Thermoelectric performance of a metastable thin-film Heusler alloy. Nature. 2019;**576**:85-90. DOI: 10.1038/s41586-019-1751-9

[95] Oliynyk AO, Antono E, Sparks TD, Ghadbeigi L, Gaultois MW, Meredig B, et al. High-throughput machine-learning-driven synthesis of full-Heusler compounds. Chemistry of Materials. 2016;**28**:7324-7331. DOI: 10.1021/acs.chemmater.6b02724

[96] Kim K, Ward L, He J, Krishna A, Agrawal A, Wolverton C. Machine-learning-accelerated high-throughput materials screening: Discovery of novel quaternary Heusler compounds. Physical Review Materials. 2018;**2**: 123801. DOI: 10.1103/PhysRevMaterials.2.123801